Biochimica et Biophysica Acta 1798 (2010) 275–285

Contents lists available at ScienceDirect

Biochimica et Biophysica Acta

journal homepage: www.elsevier.com/locate/bbamem

Backbone conformational flexibility of the lipid modified membrane anchor of the human N-Ras protein investigated by solid-state NMR and molecular dynamics simulation

Alexander Vogel [a,*], Guido Reuther [b], Matthew B. Roark [c], Kui-Thong Tan [d], Herbert Waldmann [d], Scott E. Feller [c], Daniel Huster [e]

[a] Junior Research Group "Structural Biology of Membrane Proteins", Martin Luther University Halle-Wittenberg, Kurt-Mothes-Str. 3, D-06120 Halle, Germany
[b] Department of Microbiology and Immunology, Albert Einstein College of Medicine of Yeshiva University, 1300 Morris Park Avenue, Bronx, NY 10461, USA
[c] Department of Chemistry, Wabash College, 301 W. Wabash Ave, Crawfordsville, IN 47933, USA
[d] Max Planck Institute of Molecular Physiology, Otto-Hahn-Str. 11, D-44227 Dortmund, Germany
[e] Institute of Medical Physics and Biophysics, University of Leipzig, Härtelstr. 16-18, D-04275 Leipzig, Germany

ARTICLE INFO

Article history:
Received 4 August 2009
Received in revised form 28 September 2009
Accepted 30 September 2009
Available online 9 October 2009

Keywords:
Membrane protein
Lipid modification
Structural dynamics
Replica exchange
Order parameter
Relaxation

ABSTRACT

The lipid modified human N-Ras protein, implicated in human cancer development, is of particular interest due to its membrane anchor that determines the activity and subcellular location of the protein. Previous solid-state NMR investigations indicated that this membrane anchor is highly dynamic, which may be indicative of backbone conformational flexibility. This article aims to address if a dynamic exchange between three structural models exist that had been determined previously. We applied a combination of solid-state nuclear magnetic resonance (NMR) methods and replica exchange molecular dynamics (MD) simulations using a Ras peptide that represents the terminal seven amino acids of the human N-Ras protein. Analysis of correlations between the conformations of individual amino acids revealed that Cys 181 and Met 182 undergo collective conformational exchange. Two major structures constituting about 60% of all conformations could be identified. The two conformations found in the simulation are in rapid exchange, which gives rise to low backbone order parameters and nuclear spin relaxation as measured by experimental NMR methods. These parameters were also determined from two 300 ns conventional MD simulations, providing very good agreement with the experimental data.

1. Introduction

More and more evidence is accumulating that the structures of soluble proteins are best represented by dynamic structural ensembles rather than a single "frozen" conformation. In particular, biological function of these molecules has been found to depend on dynamic processes that include less populated excited states out of an ensemble of the highly populated ground state. Such processes have recently received much attention as NMR and other methods have been developed to study such events [1,2]. Interestingly, membrane proteins can also be remarkably mobile molecules [3-7] that reside in a membrane environment formed by lipids. Recent research has shown that the membrane represents a highly dynamic assembly of flexible molecules providing the most appropriate environment for membrane protein function [8,9]. In addition to transmembrane proteins that for instance constitute channels or receptors, peripheral membrane proteins are responsible for numerous biological functions in signal transduction. One such peripheral membrane protein is the lipid modified Ras.

Ras proteins constitute a small class of GTP binding proteins, which are of great interest due to their association with cancer development [10]. The membrane binding domains of Ras proteins are of particular interest as membrane association is crucial for protein activity [11,12]. Pharmacological approaches aiming to influence Ras function, for example, are typically based on alteration of the membrane association [13,14]. The soluble N-terminal G domain shows highest homology between the four members of the Ras family, while significant differences are observed in the C-terminal region. In this hypervariable region of 23 or 24 amino acids, the homology is less than 15% [15,16]. This region also features the membrane anchor of Ras, which may consist of three lipid modifications (H-Ras), two lipid modifications (N-Ras and K-Ras4A), or one lipid modification in combination with a cluster of basic amino acids (K-Ras4B) [17]. Since all Ras isoforms interact with the same effectors *in vitro* but provide

Abbreviations: DIPSHIFT, dipolar coupling and chemical shift; DMPC, 1,2-dimyristoyl-phosphocholine; FSLG, frequency-switched Lee-Goldburg; GTP, guanosine triphosphate; MAS, magic-angle spinning; MD, molecular dynamics; NMR, nuclear magnetic resonance; NOE, nuclear Overhauser enhancement; PAS, principle axis system; TALOS, torsion angle likelihood obtained from shift and sequence similarity; TMS, tetramethylsilane

* Corresponding author. Tel.: +49 0 345 55 24942; fax: +49 0 345 55 27013.
E-mail address: alexander.vogel@biochemtech.uni-halle.de (A. Vogel).

0005-2736/$ – see front matter © 2009 Elsevier B.V. All rights reserved.
doi:10.1016/j.bbamem.2009.09.023

different output signals *in vivo*, these biological differences must be imparted by the alteration in the hypervariable region [18]. Further, the distribution of Ras between liquid crystalline and raft domains of the plasma membrane [16] and the life time in various cellular membranes [19] is thought to be highly important for the biological function of Ras. All these topics involve the Ras anchoring domain, its lipid modifications, and their interaction of with the membrane.

Until recently, very little structural and dynamical data was available to base understanding of the interesting membrane structural biology of Ras. Progress in the synthesis strategies of lipidated proteins [20,21] as well as advanced solid-state NMR technologies [22,23] have provided more insights into the structure and dynamics of the Ras membrane anchor. Using these innovations, we recently described a first structural model of the membrane anchor of the entire N-Ras protein [24] and quantitatively characterized the molecular dynamics of this protein region bound to lipid membranes [25]. In these studies, structural information was obtained from isotropic chemical shifts determined from ^{13}C and ^{1}H magic-angle spinning (MAS) NMR data. Modern data base approaches can convert chemical shift information into structural data and vice versa [26-28]. Though typically rather precise, the relationship between chemical shift and secondary structure is not always unambiguous. In the determination of the Ras structural model the chemical shift data converged into a single set of backbone torsion angles for all amino acids except for Met 182, where three rather equally populated conformations were predicted [24] by the TALOS database approach [26]. This situation is illustrated in Fig. 1, which shows the backbone torsion angle distributions for Met 182 determined from TALOS. To be most objective, three sets of structures were calculated (Fig. 1B–D) and the final model was selected based on intermolecular protein-membrane NOEs [29,30].

Nevertheless, the question remains if the structural degrees of freedom of the Ras membrane anchor implied by the three sets of torsion angles found for Met 182 represent conformers that are populated with a lesser probability or just denote false predictions from the TALOS database. Previous short MD simulations have also indicated structural flexibility in the Ras membrane anchor [31]. To better understand this issue, we carried out MD simulations that were accompanied by additional experimental NMR investigations, a combination that has lately been used increasingly often as highly complementary techniques [32-35]. MD simulations provide an atomistic picture in an all atom representation on a time frame of up to hundreds of nanoseconds. Thus, not only backbone torsion angles can be observed for the peptide but also its conformational dynamics, i.e. interconversion between conformational states. Further, the simulations allows for an analysis of the peptide structure in terms of correlations within the entire backbone while the structure prediction programs typically only consider the influence of the directly neighboring amino acids in a structure. In addition, we analyzed the molecular dynamics of the membrane bound peptide from NMR relaxation experiments and measurements of the motionally averaged dipolar couplings [36,37], allowing direct comparison with the fast motions of the molecule observed in the MD simulations. Thus, a rather comprehensive image of the dynamic conformation of the Ras membrane anchor emerges.

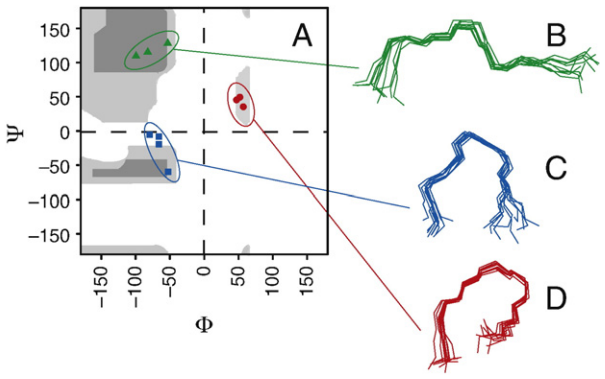

Fig. 1. The backbone structure of the membrane anchor of the human N-Ras protein was previously predicted by measurement of ^{1}H and ^{13}C chemical shift values and subsequent analysis by TALOS. While all other amino acids exhibited a dominant cluster of torsion angle pairs, Met 182 exhibited three similarly populated states, which are shown in a Ramachandran diagram in panel A (sterically allowed torsion angle ranges are indicated in grey). From the obtained torsion angles, three families of structures were predicted and the ten lowest energy backbone structures of each are shown in B, C, and D. Based on other available experimental data, the structure family shown in D was considered to constitute the most likely conformation.

2. Materials and methods

2.1. Sample preparation

1,2-Dimyristoyl-sn-glycero-3-phosphocholine (DMPC) was procured from Avanti Polar Lipids (Alabaster, AL) and used without further purification. Protected amino acids and coupling reagents were obtained from Novabiochem (La Jolla, CA) and Fmoc protected U-$^{13}C/^{15}N$ labeled amino acids were purchased from Euriso-Top (Saarbrücken, Germany) The Ras peptide with the amino-acid sequence H-Gly-Cys(HD)-Met-Gly-Leu-Pro-Cys(HD)-OMe was synthesized following Hinterding et al. [38], Nägele et al. [39], and Schelhaas et al. [40]. HD means a hexadecyl thioether. The peptide was uniformly ^{13}C and ^{15}N labeled. Aliquots of Ras peptide and phospholipid (1:10 molar ratio) were combined in chloroform, dried using a rotary evaporator, and then dissolved in cyclohexane. After freezing in liquid nitrogen, the samples were lyophilized under a vacuum of approximately 0.1 mbar. Subsequently, the sample was hydrated to 35 wt% with deuterium-depleted $^{1}H_2O$ buffer (10 mM HEPES, 10 mM NaCl, 1 mM $MgCl_2$, pH 7.4), freeze–thawed, stirred, and gently centrifuged for equilibration. They were then transferred into 4 mm MAS rotors with Teflon insert.

2.2. MAS NMR spectroscopy

All MAS NMR experiments were carried out on the Avance 750 spectrometer at resonance frequencies of 749.8 MHz for ^{1}H and 188.5 MHz for ^{13}C using a double-resonance MAS probe equipped with a 4 mm spinning module. Chemical shifts were referenced relative to TMS. ^{13}C cross-polarization MAS spectra were acquired using a 4 μs ^{1}H 90° excitation pulse and a contact time of 0.7 ms. The strength of the ^{1}H–^{13}C dipolar couplings was measured using the constant time dipolar and chemical shift (DIPSHIFT) pulse sequence [41]. ^{1}H–^{1}H homonuclear decoupling was achieved with the frequency-switched Lee–Goldburg (FSLG) sequence [42]. Since the dipolar-induced signal decay is periodic, it was only necessary to acquire the signal over one rotor period in the indirect dimension. The time evolution of the C–H dipolar couplings in 2D DIPSHIFT experiments was simulated for one rotor period [41]. Simulations were performed for varying dipolar coupling strengths with powder averaging in 2° increments for the β and γ Euler angles. Order parameters were determined as the ratio of motionally averaged and full dipolar coupling, determined for rigid amino acids [43].

^{13}C MAS T_1 and T_2 relaxation times were measured using standard pulse sequences. Typical ^{13}C π/2 pulse lengths were 5 μs. The temperature dependence of the relaxation times was simulated using a modified Lipari–Szabo approach [44] with an Arrhenius temperature dependence of the correlation times with $\tau_0 = 10^{-15}$ s [45]. It was further assumed that any hydrogens directly bonded to the $^{13}C\alpha$ relax its spin. Anisotropic interactions are modeled both for the fast (f) and the slow (s) peptide motions while the overall isotropic reorientation of the peptide was assumed to be inhibited by the

presence of the membrane and the corresponding correlation time τ_R was set to infinity. The spectral density functions are then given by [44]

$$j(\omega) = \frac{1}{5}\left[\frac{\left(1-S_f^2\right)\tau_f}{1+(\omega\tau_f)^2} + \frac{\left(S_f^2-S^2\right)\tau_s}{1+(\omega\tau_s)^2}\right], \quad (1)$$

where the fast motions are described by the order parameter S_f and the correlation time τ_f while S_s and τ_s describe the slow motions. The overall order parameter is the product of the two individual order parameters $S = S_f \times S_s$ and the experimentally determined DIPSHIFT order parameter was used for it to reduce the number of fitting parameters in the model.

2.3. MD simulations

All simulations consisted of four Ras peptides, 40 DMPC lipids, and 984 waters. Setup of the membrane was conducted following published procedures [46]. Two peptides were added to each monolayer of the membrane and aligned according to previously determined experimental data [30]. The starting configuration of the peptide backbone was taken from the experimentally determined backbone structure [24]. Subsequently, pre-equilibrated lipids were randomly picked and homogeneously distributed in the plane of each monolayer. Initially, the surface area was estimated from the previously published experimentally measured deuterium order parameters of the lipids and peptides [30] and the relation between order parameters and molecular surface area [47]. During equilibration the order parameters of the lipids slightly deviated from the ones measured experimentally so that the area was adjusted until the order parameters from simulation and experiment agreed. The program CHARMM [48] was employed for the simulation and its analysis, using the CHARMM all-H CMAP protein force field [49,50] with the all-H lipid force field, including a recent refinement of the saturated acyl-chain torsions [51]. The smooth particle-mesh Ewald algorithm was used to compute the electrostatic forces [52] and the SHAKE algorithm was used to maintain rigid all bonds involving hydrogen atoms, allowing a 2 fs time step [53]. All simulations were run under conditions of constant surface area and normal pressure (1.013 bar).

A replica exchange technique was employed to enhance sampling of the backbone conformations [54-57]. In total, 34 replicas were simulated at temperatures ranging from 303 K to 514 K. Spacing of the temperatures was adjusted such that the probability to accept a swap of replicas in neighboring temperatures was ~10%. The simulation reported followed an equilibration replica exchange simulation that was run for 54.2 ns. The production simulation was continued for 39.2 ns and all data presented here were taken from the lowest temperature bath at 303 K.

Two conventional MD simulations of 300 ns length each were also conducted to allow calculation of correlation functions. The starting configurations were taken from two independent replicas in the lowest temperature bath at the end of the replica exchange simulation. An additional equilibration of 5 ns was conducted before the start of the production run.

Analysis of the simulations included several comparisons with experimental data. Since the necessary calculations are relatively complicated and rather rarely shown explicitly for MD simulations a short summary is given here. The analysis included the calculation of ^{13}C T_1 and T_2 relaxation times, which were obtained via the discrete P_2 correlation function g of the corresponding C–H bonds that is defined as

$$g(n\Delta t) = \frac{G_0(n\Delta t) + 2G_1(n\Delta t) + 2G_2(n\Delta t)}{5}, \quad (2)$$

where Δt is the distance between neighboring points and n the running index. The individual $G_m(n\Delta t)$ are defined as

$$G_m(n\Delta t) = \frac{4\pi}{5}\left(\langle Y_{2m}(j,\vartheta,\varphi)Y_{2m}^*(j-n\Delta t,\vartheta,\varphi)\rangle_j - |\langle Y_{2m}(k,\vartheta,\varphi)\rangle_k|^2\right), \quad (3)$$

where averaging is performed over all possible indices j and k. Here the well known spherical harmonics $Y_{2m}(n\Delta t, \vartheta, \varphi)$ are used, which are calculated using the spherical coordinates (ϑ, φ) of the C–H bond vector at the time point $n\Delta t$ that can be directly extracted from the MD simulation. The Fourier transform of the P_2 correlation function is the spectral density function $j(\omega_k)$, which is also discrete and defined as

$$j(\omega_k) = 2\sum_{n=0}^{l-1} g(n\Delta t)\cdot\cos(\omega_k \cdot n\Delta t)\Delta t, \quad (4)$$

where l is the number of points in the correlation function and the discrete frequencies are defined as

$$\omega_k = 2\pi\frac{k}{l\Delta t}. \quad (5)$$

Many mathematics packages include predefined functions with superior performance for calculating correlation functions and Fourier transforms but special care has to be applied since they often use different prefactors. Subsequently, the spectral density is sampled at various frequencies to facilitate the calculation of T_1 and T_2 relaxation times via

$$\frac{1}{T_1} = n_H\pi^2\chi_D^2\left(j(\omega_H-\omega_C)+3j(\omega_C)+6j(\omega_H+\omega_C)\right)+\left(\frac{\omega_C\Delta\sigma}{\sqrt{3}}\right)^2 j(\omega_C)$$

$$\frac{1}{T_2} = \frac{n_H\pi^2\chi_D^2}{2}\left(4j(0)+j(\omega_H-\omega_C)+3j(\omega_C)+6j(\omega_H)+6j(\omega_H+\omega_C)\right) + \left(\frac{\omega_C\Delta\sigma}{\sqrt{18}}\right)^2\left(4j(0)+3j(\omega_C)\right) \quad (6)$$

where χ_D is the dipolar coupling constant (which has a value of 22.7 kHz for a ^{13}C–^{1}H bond), $\Delta\sigma$ is the span of the chemical shift anisotropy tensor (which has a value of 37 ppm for Gly and Pro, 24 ppm for Met, 38 ppm for Leu, and 29 ppm for Cys [58]), n_H is the number of hydrogens bound to the ^{13}C atom, and ω_X is the Lamor frequency of the nucleus X at the investigated magnetic field strength.

Calculating relaxation times from MD simulations by this formalism poses several technical problems. First, the correlation function typically becomes very noisy at the end due to insufficient sampling, which upon Fourier transformation refolds into the spectral density, which then becomes noisy as well. To reduce this problem we fitted the correlation function to a set of exponentials [59] and replaced the noisy long time tail by the fit (one has to be careful to switch from the true correlation function to the fit in a point where both are very close to each other since any discontinuity leads to artifacts in the spectral density). Second, the correlation function and spectral density will be discrete for MD simulations, which might lead to considerable errors in the frequencies, at which the spectral density is sampled for calculation of the relaxation times. To circumvent this problem it is useful to cut a few points at the end of the correlation function before Fourier transformation to change the spacing of points in the spectral density (the distance between neighboring points in $j(\omega_k)$ is $2\pi/l\Delta t$).

Another scarcely described procedure is the prediction of DIPSHIFT order parameters from MD simulations. For this, first the tensor of the dipolar interaction has to be averaged over all simulation frames. In

the principal axis system this tensor is diagonal and has the general matrix representation

$$\mathbf{D}^{\mathrm{PAS}} = \begin{pmatrix} D_{xx} & 0 & 0 \\ 0 & D_{yy} & 0 \\ 0 & 0 & D_{zz} \end{pmatrix}, \tag{7}$$

where for a ^{13}C–^{1}H bond $D_{xx} = D_{yy} = -11.35$ kHz and $D_{zz} = 22.7$ kHz. Since this tensor is expressed in the PAS, whose largest component is aligned along the C–H bond a coordinate transformation to a fixed system has to be conducted for each simulation frame using

$$\mathbf{D}^{\mathrm{fixed}} = \mathbf{R}^{-1}(\alpha,\beta,\gamma)\mathbf{D}^{\mathrm{PAS}}\mathbf{R}(\alpha,\beta,\gamma), \tag{8}$$

where $\mathbf{R}(\alpha, \beta, \gamma)$ denotes the well known Euler rotation matrix with the Euler angles α, β, and γ. When performing this rotation, one has to be careful to distinguish between passive and active rotations as α, β, γ, and $\mathbf{R}(\alpha, \beta, \gamma)$ are differently defined for the two cases [60]. Subsequently, the interaction tensor in the fixed frame $\mathbf{D}^{\mathrm{fixed}}$ is averaged over all time steps of the simulation. It might also be useful to average the interaction tensor over several molecules (instead of averaging over their individual order parameters at the end) since this can reduce the difference in the time scales of the DIPSHIFT experiment (a few microseconds) and the simulation (hundreds of nanoseconds). This way motions not completely sampled for a single molecule of the simulation (e.g. axial reorientation) can artificially be introduced and contribute to the reduction of the DIPSHIFT order parameter. However, one has to be careful when doing this as it has to be certain that the molecules, over which are averaged exchange on the timescale of the DIPSHIFT experiment. For instance, one should usually not average over molecules in different leaflets of the bilayer unless flip-flop occurs on the timescale of the DIPSHIFT experiment, which is unlikely for most membrane molecules. The average tensor is then diagonalized by calculation of the eigenvectors, assembling them into a rotation matrix $\mathbf{R}_2$ by using each eigenvector for one column and subsequent coordinate transformation using

$$\mathbf{D}^{\mathrm{diagonal}} = \mathbf{R}_2^{-1}\langle\mathbf{D}^{\mathrm{fixed}}\rangle\mathbf{R}_2. \tag{9}$$

The largest principal component of $\mathbf{D}^{\mathrm{diagonal}}$ is then put into proportion with D_{zz} such that the DIPSHIFT order parameter is defined as $S_{\mathrm{DIPSHIFT}} = \max(|D_{xx}^{\mathrm{diagonal}}|, |D_{yy}^{\mathrm{diagonal}}|, |D_{zz}^{\mathrm{diagonal}}|)/D_{zz}$.

3. Results

3.1. Structural variability of the Ras backbone

The backbone torsion angles of the seven amino acid membrane anchor of the human N-Ras protein were previously determined from ^{1}H and ^{13}C chemical shifts using TALOS [26], which lead to a first structural model determined by solid-state NMR [24]. However, the relation between isotropic chemical shifts and secondary structure was ambiguous for Met 182 (Fig. 1). Fortunately, for all other amino acids TALOS provided conclusive results for Φ, Ψ pairs. Since TALOS is a pure database approach a simulated annealing protocol was used to generate the resulting structures. The three different sets of Met 182 Φ, Ψ pairs were treated independently such that the simulated annealing was conducted for all of them and the resulting ten lowest energy backbone structures are shown in Fig. 1B–D.

In the original article [24] additional structural constraints determined in previous investigations [29,30] were used to select one structure, which agreed with all available data and therefore represented the most likely model of the Ras backbone structure (ref. Fig. 1D). Here, we seek to learn if the three conformations that resulted from the ambiguity of the TALOS results for Met 182 would represent populated structures or were solely caused by the non-perfect correlation between chemical shift and secondary structure. To this end, we conducted MD simulations, which allow to directly observe the backbone torsion angles and to identify different conformers if present. For these simulations the structural model determined previously was used to generate the starting configuration [24]. Since conventional simulation approaches did not result in sufficient sampling of the backbone torsions [31,61] the replica exchange technique was used here with temperatures ranging from 303 K to 514 K. A Monte Carlo procedure is applied periodically to swap configurations among the various temperatures, thus each replica spends time at higher temperatures allowing transitions over high energy barriers, which is unlikely to happen at the temperature of primary interest. Therefore, the rate of transitions for the backbone torsion angles is significantly increased leading to much more efficient sampling [55,56].

Histograms of the backbone torsion angles Φ and Ψ were calculated for all amino acids. Some of them exhibit a narrow distribution, while others are distributed over a wide range of angles or show several separate maxima. Two typical examples are shown in Fig. 2. In general, most torsion angles show a rather large variation indicating that the structure of the backbone is rather flexible. To obtain a better picture of the flexibility and to allow for a straightforward comparison with the experimentally determined values, 2D Ramachandran diagrams of the Φ, Ψ torsion angles were calculated for the five inner amino acids (Fig. 3). These diagrams exhibit several maxima for all five amino acids also indicating a flexible backbone. However, most of the structural heterogeneity is observed for the N-terminal amino acids while the structure of the C-terminus is better defined. This is in agreement with the previous experimental observation that the amino acids at the C-terminus show larger deviations from the NMR isotropic chemical shift value [24] indicating that less averaging occurs for them. Additionally, the comparison of the torsion angles from simulation and experiment shows very good agreement. The major clusters from the TALOS predictions (which are indicated by symbols in Fig. 3) with one exception always overlap with the maximum observed in the simulations. The only exception of this is Cys 181, which is not very surprising as one of the lipid modifications is attached to its side chain. The very strong hydrophobic interaction of this lipid modification with the membrane most likely shifts the energy minimum to a different set of torsion angles, which cannot be predicted by TALOS as information neither about the lipid modifications nor the membrane environment is included in its database approach. Using the HNCH

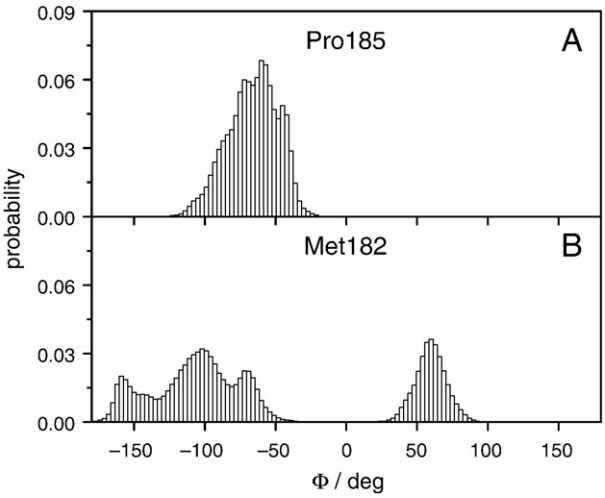

Fig. 2. Histograms of the backbone torsion angle Φ of Pro 185 (A) and Met 182 (B) determined from the replica exchange simulation. Data were taken from the lowest temperature bath (303 K) of the replica exchange simulation. While the histogram for Φ of Pro 185 shows a single conformation Φ of Met 182 exhibits four distinct maxima indicating large structural flexibility of the peptide backbone in this region.

experiment [41], Φ torsion angles were also determined experimentally (data not shown). The two values, which could be unambiguously assigned to Met 182 ($-91°\pm31°$) and Leu 184 ($-100°\pm20°$), convincingly overlap with the Ramachandran diagrams from the simulation.

The observation of several maxima in the Ramachandran diagrams can be interpreted in two ways: either the backbone is very flexible in general, e.g. with little or no correlation between the torsional states of the various amino acids, or a small set of different structures exists. If the latter was true individual amino acids would change their torsion angles collectively, while they would be independent in the first case. To distinguish between these two possibilities further inter-residue Ramachandran diagrams were calculated, where any Φ or Ψ angle was correlated with any Φ or Ψ angle of any amino acid. Two types of these inter-residue Ramachandran diagrams were calculated: (i) The inter-residue Ramachandran diagram was predicted from the 1D histograms of the two torsion angles by simple multiplication (ref. Fig. 2), which explicitly includes the assumption that they are uncorrelated. (ii) The inter-residue Ramachandran diagram was calculated directly from the simulation, which would contain correlations between the amino acids whose torsion angles are analyzed. If the two types of diagrams are the same for a given pair of torsion angles these angles are uncorrelated while they are correlated if the diagrams differ considerably.

Two examples of this analysis are shown in Fig. 4, where the inter-residue Ramachandran diagrams that were predicted assuming uncorrelated torsion angles are shown in Fig. 4A and D, while the ones directly calculated from the simulation are shown in Fig. 4B and E. The differences A–B and D–E are shown in Fig. 4C and F, respectively. As can be seen from this example the Φ of Leu 184 and the Ψ of Pro 185 are virtually uncorrelated. In contrast, the Φ of Cys 181 depends strongly on the Φ of Met 182. When the Φ of Met 182 is about 60° the Φ of Cys 181 is almost always about −160°, while it is about −70° when the Φ of Met 182 is negative. The same analysis was conducted for all possible combinations of torsion angles and a correlation score calculated. The correlation score is defined as the sum of the absolute values of all data points in the difference diagram (for examples see Fig. 4C and F) and has a theoretical maximum of 2.0 if there is no overlap between the two types of inter-residue Ramachandran diagram. However, in reality there will always be considerable overlap, which leads to scores on the order of 0.5 to 1.0 for intra-residue Ramachandran diagrams, which are typically strongly correlated. The correlation scores for the entire backbone are shown in Fig. 5. From this, it is evident that there is strong correlation between the different torsion angles at the N-terminus of the backbone (Cys 181 and Met 182 in particular), while they are only loosely correlated in the C-terminus. This is partly due to the fact that some torsion angles at the C-terminus only exhibit a narrow distribution of values and, therefore, do not show structural variability at all.

The strong correlation between the torsions of the N-terminal amino acids clearly indicates that the observed structural flexibility is due to the existence of a number of different structures, which exchange at the higher temperatures of the replica exchange simulation. To investigate the present structures a cluster analysis of all torsion angle time series was performed for the Ras backbone (Fig. 6). In total 17 clusters (of which 5 were below 0.3% probability) were found and the two major conformations account for ~34% and ~26% of the simulation time (all others were below 10%). The difference between these two structures is mainly located at the N-terminus of the peptide and in particular amino acids Cys 181 and Met 182 seem to play the major role in defining the structure of the peptide. Some of the minor conformers agree with the most common conformer in these crucial amino acids and only differ in the C-terminal part of the peptide that is characterized by uncorrelated structural flexibility (see Fig. 5). If these minor conformers are assumed to be merely fluctuations of the most common conformer the two major conformers constitute ~77% of all the structures observed in the simulation.

In Fig. 7, the average structures of the two major conformers are aligned with respect to the experimental structure from Fig. 1D. This comparison clearly shows that the experimental structure (grey) is very similar to the average structure of cluster 2 (blue), while the structure of cluster 1 (red) exhibits a kink in Met 182, which leads to a different conformation of the N-terminus. At the same time, the conformation of Cys 181 is also different between cluster 1 and

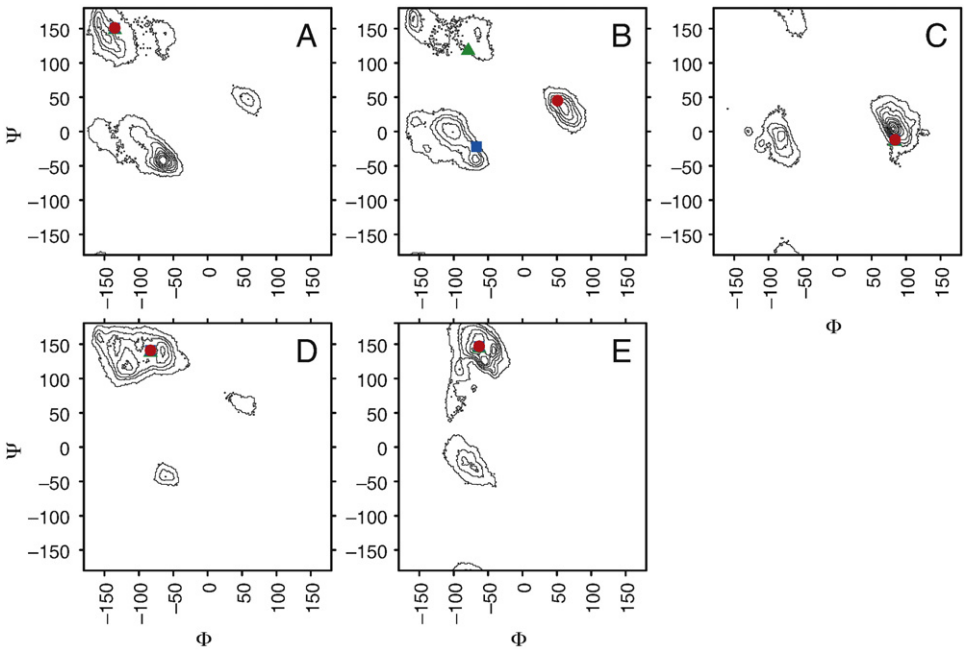

Fig. 3. Ramachandran diagrams of the five inner amino acids Cys 181 (A), Met 182 (B), Gly 183 (C), Leu 184 (D), and Pro 185 (E) of the peptide. Data were taken from the lowest temperature bath (303 K) of the replica exchange simulation. All diagrams exhibit several maxima indicating the structural flexibility of the peptide backbone. The torsion angles of the three structures from Fig. 1B (green triangles), C (blue squares), and D (red circles) are also indicated.

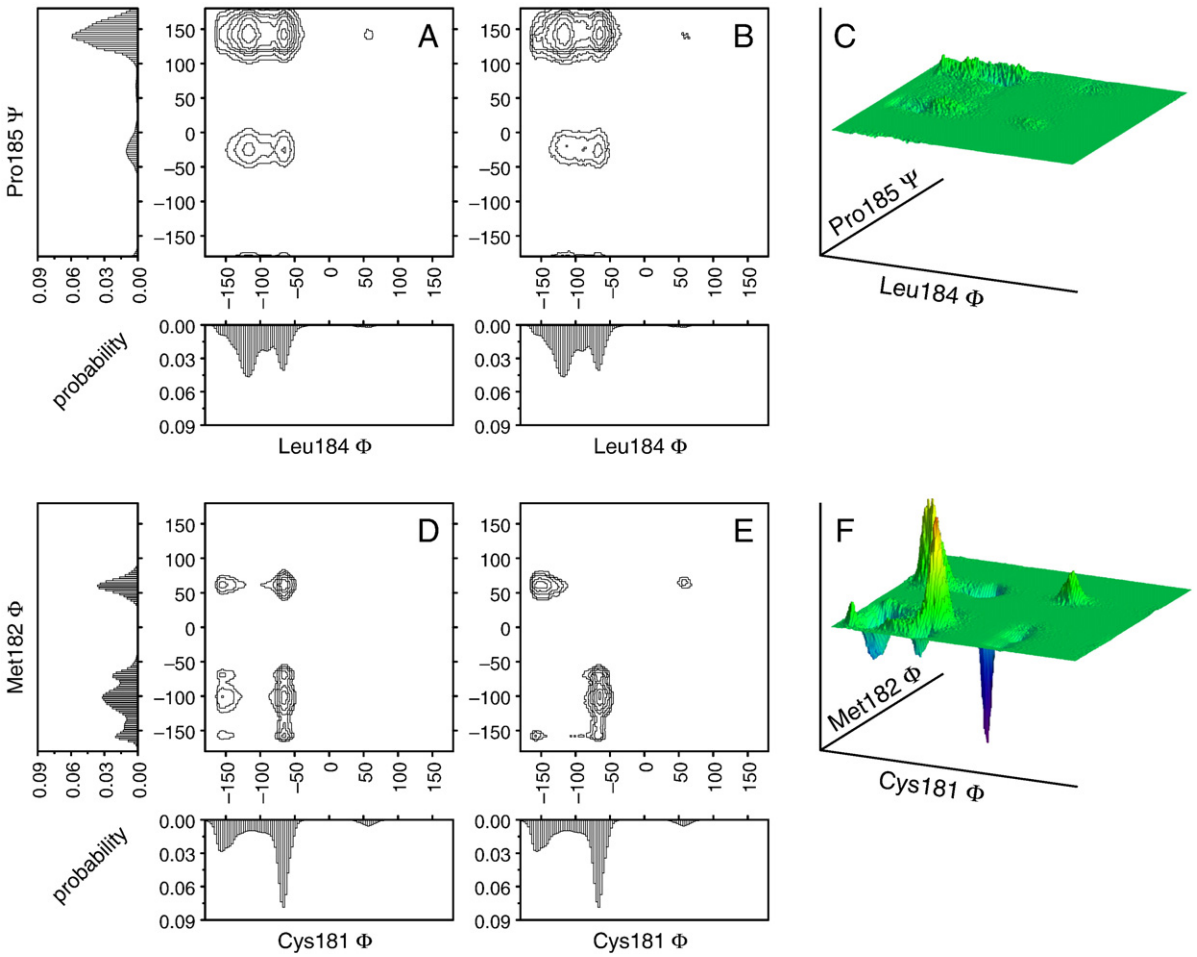

Fig. 4. Schematic representation of the correlation analysis. Inter-residue Ramachandran diagrams predicted from the one dimensional histograms of two torsion angles assuming no correlation between them are shown for the Leu 184 Φ and Pro 185 Ψ pair (A) and for the Cys 181 Φ and Met 182 Φ pair (D). The corresponding diagrams evaluated directly from the lowest temperature bath (303 K) of the replica exchange simulation are shown in B and E, respectively. Subtraction of the two types of diagrams (results shown in C and F) allows assessing if the two torsion angles are correlated. If the subtraction diagram is very flat as shown in C the two torsion angles are uncorrelated, while they are correlated if the subtraction diagram shows pronounced minima and maxima as shown in F.

cluster 2. This is most likely due to the lipid modification that would otherwise not be well embedded into the bilayer while the polar NH_2 group at the N-terminus would penetrate the hydrophobic

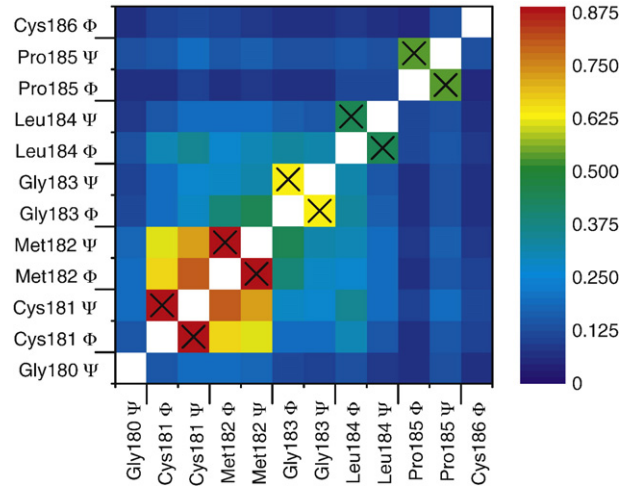

Fig. 5. Summary of the correlation analysis for the entire Ras backbone. The correlation scores are color coded and shown for each torsion angle pair. Torsion angle pairs belonging to the same amino acid which are naturally highly correlated are indicated by black × symbols.

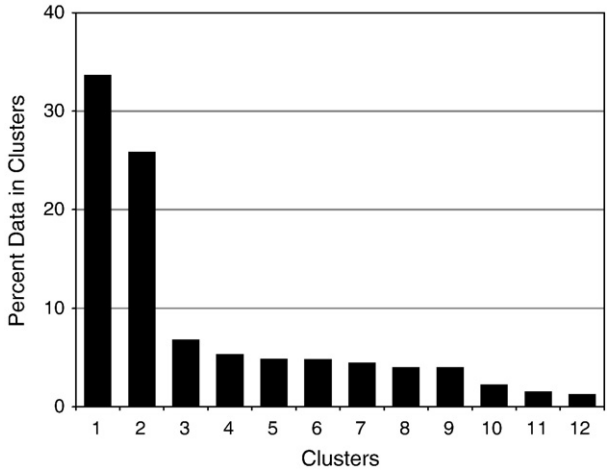

Fig. 6. Result of the cluster analysis of the torsion angle time series from the lowest temperature bath (303 K) of the replica exchange simulation. The cluster analysis was performed for all four peptides together and a total of 17 clusters was found of which 12 are shown (the other 5 clusters are below 0.3% probability). The two major clusters constitute 60% of all structures while all other clusters remain below 10%. Clusters 3, 5, 8, and 12 are identical to cluster 1 in the torsions of Cys 181 and Met 182, which are most important for the structure.

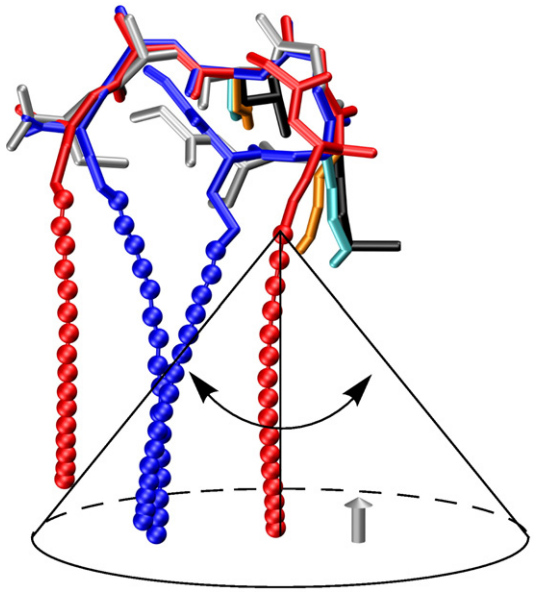

Fig. 7. Comparison of the experimentally predicted backbone structure from Fig. 1D (grey) and the average backbone structures of the two major clusters (cluster 1: red, cluster 2: blue). The C-terminus of the peptide is on the left side and the orientation of the membrane normal is indicated by the grey arrow in the lower right of the picture. The hydrophobic side chains of Met 182 and Leu 184 are shown in black for the experimental structure, orange for cluster 1, and cyan for cluster 2 (Leu 184 is in the middle of the picture while Met 182 is closer to the right side) and the lipid modification carbons are shown in a ball and stick representation. It is noteworthy that the lipid modifications are highly flexible which is indicated for one of them by the cone angle of its slow motion.

region of the bilayer. In fact the average structures of the two clusters feature a topology, in which the hydrophobic side chains of Met 182 and Leu 184 and also the side chains of Cys 181 and Cys 186, to which the lipid modifications are attached, are all facing one side of the peptide, which is always facing the membrane in the MD simulations. It is interesting to note that the Leu 184 side chain is pointing somewhat sideways, while all other hydrophobic moieties are almost perfectly aligned but the reason for this alignment remains unclear from the investigations presented here. This is in very good agreement with a previously obtained model of the topology of the peptide and this observation was actually used to identify the structure in Fig. 1D as the one, which is most likely correct because the other two structures (Fig. 1B and C) do not exhibit this topology [30].

Nevertheless, these two structures were aligned with respect to the average structures of cluster 1 and 2 as well (data not shown) but no good agreement could be found. The reason for this is the collectivity of structural changes in the torsion angles of Cys 181 and Met 182, which means that a change in Met 182 must always be accompanied by a change in Cys 181. While TALOS was able to correctly predict diverse conformations in Met 182 it could not predict the diversity in Cys 181 and, therefore, led to these two structures not observed in the simulation.

3.2. Dynamical flexibility of the Ras backbone

An interesting dynamic behavior of the peptide is already suggested from its structural variations and flexibility. In addition, former investigations revealed that the Ras lipid modifications are characterized by large amplitude motions [25,61,62]. Since the dynamics of the membrane anchor is most likely of high importance for the binding to the highly flexible membrane and perhaps even for its subcellular location additional solid-state NMR experiments and two independent conventional MD simulations were conducted. In particular, the dynamic fluctuations of the Cα–H bond were investigated as they are directly connected to the peptide backbone and experimentally accessible.

The DIPSHIFT order parameters of this bond were measured by determination of the motionally averaged ^{13}C–^{1}H dipolar coupling and are shown in Fig. 8 (grey bars). The absolute values for these order parameters are very low indicating large amplitude motions in the backbone of the Ras membrane anchor. For the five inner amino acids, a clear trend is observed, in which the order parameters rise monotonically towards the C-terminus, which also exhibited less structural heterogeneity in the Ramachandran diagrams. Compared to values obtained for full-length N-Ras the ones obtained here are somewhat smaller, which can be explained by the missing soluble part of the protein that dampens the motions of the membrane anchor if present [25]. Interestingly, the order parameters determined for Cys 181/186 (which cannot be distinguished due to signal overlap), to which the lipid modifications are attached, are the lowest for the whole peptide which is likely connected to the high amount of flexibility observed for the lipid modifications [61,62]. In addition, the order parameter for Met 182 is almost as low, leading to the result that the DIPSHIFT order parameters of the amino acids, which are most strongly correlated in the MD simulation are the lowest in the whole backbone.

The DIPSHIFT order parameters were also calculated from the replica exchange simulation and are shown in Fig. 8 as well (white bars). It is important to note that the calculation is different from calculating ^{2}H NMR order parameters since the average orientation of the C–H bond vector is in general not perpendicular to the membrane normal. Therefore, the complete tensor had to be considered and averaged over all frames. The comparison of the obtained order parameters shows reasonable agreement with the experiment in particular for the five inner amino acids, where even the general trend is reproduced rather well. The observation that the order parameters from the simulation are generally higher than the ones measured experimentally likely arises from the fact that DIPSHIFT order parameters are also sensitive to motions with correlation times that are much longer than the total time of simulations conducted in this article.

To assess the backbone dynamics in more detail, ^{13}C NMR relaxation times measured as a function of temperature of the sample are shown in Fig. 9. Generally, the T_1 relaxation times decrease with increasing temperature while the T_2 relaxation times increase, which

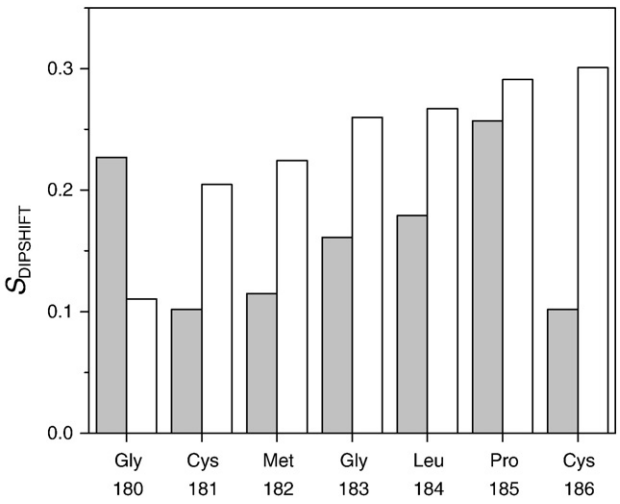

Fig. 8. Comparison of the DIPSHIFT order parameters determined from simulation (white) and experiment (grey). They were evaluated from the lowest temperature bath (303 K) of the replica exchange simulation and determined experimentally at $T = 303$ K using the DIPSHIFT method at a MAS frequency of 3.5 kHz respectively. The experimental DIPSHIFT order parameters for Cys 181 and Cys 186 are identical because they could not be distinguished in the NMR spectrum.

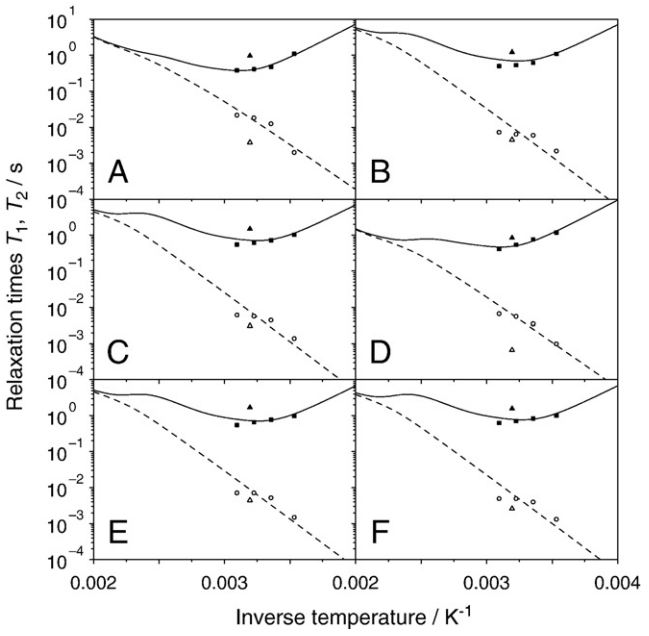

Fig. 9. Semilogarithmic representations of the T_1 and T_2 relaxation times in dependence on the inverse temperature for Gly 180 (A), Cys 181/186 (B), Met 182 (C), Gly 183 (D), Leu 184 (E), and Pro 185 (F). Experimental values are indicated by black squares for T_1 and white circles for T_2 while the theoretical fits using Eqs. (1) and (6) are shown as solid and dashed lines respectively (for each amino acid the T_1 and T_2 relaxation times were fitted simultaneously). The relaxation times obtained from the conventional MD simulations at 313 K are indicated by black triangles for T_1 and white triangles for T_2.

is typical for motions not in the extreme narrowing limit. By fitting the data with a modified Lipari–Szabo approach [44], correlation times of the motions could be determined. In this model, the spectral density contains three terms describing two independent anisotropic motions and the overall reorientation of the peptide. Here however it was assumed that the overall isotropic reorientation of the peptide is inhibited by the presence of the membrane and the corresponding correlation time τ_R was set to infinity. The anisotropy of the fast and slow motions is represented in the order parameters S_f and S_s. To reduce the number of fitting parameters it was assumed that the experimentally measured DIPSHIFT order parameter is influenced by both motions and can therefore be expressed as $S_{DIPSHIFT} = S_f \times S_s$ [44]. For the temperature dependence of the correlation times an Arrhenius behavior was assumed, which is modeled in the activation energies of the two motions. This leaves three parameters for the fit, one order parameter and the two activation energies. The resulting fits reproduce the data very well and the resulting correlation times for the fast and slow motions of the peptide are summarized in Tables 1 and 2. At room temperature the correlation times for the fast motions τ_f are on the order of 1 ns while they are on the order of hundreds of ns for slow motions of the peptide τ_s. Of course, T_1/T_2 relaxation times are not sensitive on this timescale and the large values for the correlation time simply indicate that the overall motions of the peptide are very slow as there is no isotropic tumbling at the membrane surface. The results are in good agreement with several previous investigations of the dynamics of the Ras membrane anchor. Previously, correlation times of Gly 183 were determined in the full-length Ras protein [25]. The correlation times obtained for the peptide and the protein are very close for the both motions indicating that the internal dynamics are virtually uninfluenced by the presence of the soluble part of the protein. Other experimental investigations on the peptide were conducted using ^{2}H NMR and analyzed with a more complex model of the peptide dynamics. In addition, there the data was also influenced by the motions of the of the lipid modifications due to the different location of the label. Nevertheless, the obtained rotational diffusion constants of 4.5×10^5 s^{-1} for rotation perpendicular and 2.1×10^9 s^{-1} for rotations parallel to the membrane normal [61] correlate remarkably well to the correlation times observed here.

Table 1
Correlation times τ_f in ns for the fast motions of the amino acids of the membrane bound lipid modified Ras peptide.

Amino acid	Relaxation measurements				MD
	283 K	298 K	310 K	323 K	313 K
Gly180	3.954	1.841	1.053	0.603	1.216
Cys181/186	2.229	1.068	0.624	0.365	7.550
Met182	2.140	1.028	0.601	0.352	17.39
Gly183	4.025	1.872	1.070	0.612	6.788
Leu184	2.080	1.000	0.586	0.343	6.133
Pro185	1.957	0.944	0.554	0.325	3.656

The values for the temperatures 283 K, 298 K, 310 K, and 323 K were obtained by application of a modified Lipari–Szabo model to experimentally measured, temperature dependent T_1 and T_2 relaxation times while the values at 313 K were obtained from the correlation functions observed in the conventional MD simulations.

Table 2
Correlation times τ_s in ns for the slow motions of the amino acids of the membrane bound lipid modified Ras peptide.

Amino acid	Relaxation measurements				MD
	283 K	298 K	310 K	323 K	313 K
Gly180	699.5	250.9	118.7	56.16	29.08
Cys181/186	3914	1288	571.6	253.9	146.3
Met182	4505	1471	649.9	287.2	242.9
Gly183	821.2	292.2	137.4	64.64	64.88
Leu184	3622	1196	532.6	237.3	119.6
Pro185	3912	1287	571.4	253.8	49.60

The values for the temperatures 283 K, 298 K, 310 K, and 323 K were obtained by application of a modified Lipari–Szabo model to experimentally measured, temperature dependent T_1 and T_2 relaxation times while the values at 313 K were obtained from the correlation functions observed in the conventional MD simulations.

From the two conventional MD simulations correlation functions of the Cα–H bond vectors were also calculated, which allows direct comparison to the experimental values by fitting with a double exponential [59]. The resulting correlation times for the fast and slow motions are summarized in Tables 1 and 2, respectively. Considering the relatively simple model the agreement with the experimentally determined values is very good, which is particularly remarkable for the slow motions since the experimental values are on the order of the simulation length.

A model free comparison of the backbone dynamics in simulation and experiment is allowed by comparison of the T_1 and T_2 relaxation times. They were extracted from the simulations by Fourier transformation of the correlation functions and subsequent sampling of the resulting spectral densities at the frequencies 0, $\omega_H - \omega_C$, ω_C, ω_H, and $\omega_H + \omega_C$. The obtained relaxation times are always relatively close to the experimental values (typically within a factor of 2.5), which is particularly surprising for T_2 as this heavily depends on $J(0)$ which is very sensitive to motions with long correlation times.

4. Discussion

According to the most recent structural model of the N-Ras membrane anchor, the peptide backbone is located in the lipid water interface of the host membrane with the lipid modifications and hydrophobic side chains penetrating the hydrocarbon membrane core [29,30,62]. The lipid modifications are extremely flexible [61,62] and ongoing research in our group shows that they adopt their length to the surrounding lipid matrix [76].

The main goal of the investigation presented here was a detailed analysis of the backbone structure and dynamics of the lipid modified membrane anchor of the human N-Ras protein. A combination of

solid-state NMR and MD simulations was used to achieve this goal. Since folding and transitions between several existing structures is too slow for conventional MD simulations a replica exchange technique was used to improve the sampling of conformations while two subsequent 300 ns simulations allowed investigation of the peptide dynamics. The combination of simulation and experiment is particularly powerful as both approaches complement each other very well. While meaningful MD simulations rely on experimental data to guide simulation setup and analysis and to validate the obtained results, many quantities are much easier to extract from simulations than from experiments. However the application of NMR techniques also offers distinct advantages as it allows the investigation of phenomena exceeding the time and length scales of MD simulations.

With this combined approach a set of structures was extracted from the replica exchange simulation and using a cluster analysis of the torsion angles two of them were identified as major conformers while all others populated less than 10% of the simulation time. One of the previously experimentally determined structures was very similar to the second most common structure of the simulation and could be refined. However, the dominant structure found in the simulation did not agree with the experimental model. In addition, it could be shown that these structures are not very rigid and exhibit a rather large conformational flexibility. This is also supported by a solution NMR investigation on full-length farnesylated H-Ras in the absence of membranes or micelles, which revealed that the residues that followed Asn 172 experience fast internal motions and are conformationally flexible [63].

From this and previous work, there are many indications that the observed structure of the Ras C-terminus is shaped by the membrane environment of the peptide, which makes it remarkable that TALOS was able to correctly predict the torsion angles for all amino acids besides Cys 181. For instance, the main difference observed in the two most common structures, which is located in Cys 181 and Met 182, can largely be explained by the location of the peptide backbone in the interface of a very polar and a very nonpolar region. We showed that these two amino acids change their conformation collectively and closer inspection of this conversion reveals that otherwise the lipid modifications would not be facing the same side of the peptide and would, therefore, be exposed to the surrounding solvent. Investigations on the thermodynamics of membrane binding of lipid modified peptides showed, however, that this would be highly unfavorable as each CH_2 group contributes -3.35 to -3.45 kcal/mol to ΔG^0 upon transfer from water to a membrane environment [64-66]. In addition, the polar NH_2 group at the N-terminus could penetrate the hydrocarbon region of the host membrane if Cys 181 and Met 182 would not change their structure in conjunction, which is also highly unfavorable. In fact, throughout the simulation, we observe that the lipid modifications as well as the hydrophobic side chains of Met 182 and Leu 184 are facing the same side of the peptide and penetrate the hydrocarbon core of the membrane, while the backbone amide protons are preferentially located in the lipid water interface and only rarely get in contact with the lipid acyl chains, all in excellent agreement with several experimental studies [29,30,61,62]. We therefore hypothesize that the observed structures are mainly shaped by the biophysical interactions of the individual moieties of the peptide with the complex environment in the lipid-water interface of a biological membrane, which features hydrophilic, hydrophobic, and hydrogen bonding groups in a very anisotropic manner. In turn, the resulting topology renders one face of the peptide very hydrophobic resulting in strong binding to the membrane interface.

Since these biophysical interactions are unspecific in contrast to intramolecular hydrogen bonds, which often stabilize backbone structures, a rather large amount of structural flexibility is observed, which also raises questions about the dynamics of the peptide backbone. Despite the existence of defined structures, which constitute about 60% of the simulation time rather large fluctuations are observed throughout the peptide backbone. The amino acids at the N-terminus undergo collective structural changes, while the amino acids at the C-terminus fluctuate mostly uncorrelated as revealed by the Ramachandran diagrams, which always exhibit several maxima. In addition, calculation of RMSD values for all structures belonging to either of the two most common structures (data not shown) shows that the hydrophobic side chains of Met 182 and Leu 184 exhibit a substantial degree of flexibility comparable to the top of the lipid modifications which have been characterized as extremely flexible in previous experimental and computational studies [30,61,62].

To assess the dynamics of the peptide backbone in more detail, DIPSHIFT order parameters and ^{13}C NMR relaxation times were determined and analyzed using a modified Lipari-Szabo approach. In general, the DIPSHIFT order parameters are very low throughout the backbone indicating large amplitude motions. This is partly due to the fact that the membrane anchor is not folded in a single rigid secondary structure motif. Interestingly, the DIPSHIFT order parameters reported for the full-length protein are on average about twice as high [25] indicating that the motions of the membrane anchor are somewhat dampened when the soluble part of the protein is present. Nevertheless, the DIPSHIFT order parameters of the membrane anchor even for the full-length protein are rather low in general when compared to other membrane proteins [3,25,67,68]. Interestingly the soluble part of the protein does not seem to influence the lipid modifications since very similar order parameters are reported for them in the absence and in the presence of the soluble part of the protein [25,30,62].

It is also interesting to compare the DIPSHIFT order parameters of the two cysteins, which are lipid modified. In the full-length protein, the order parameter for Cys 181, which was palmitoylated, was also comparatively low, while the order parameter of Cys 186, which was farnesylated, was the highest [25]. This difference was attributed to the difference in lipid modification mobility. This observation was important insofar as very little is known about farnesyl lipid modifications. It is reported that its free energy of transfer from water to a lipid bilayer is comparable to that of a myristoyl chain [69] and a few investigations suggested that it is mostly extended [70] and does not influence the chain order of the host membrane [71], which agreed with the observation of a higher order parameter at the cystein, to which the farnesyl chain is attached. In this study, a peptide was used, that featured hexadecylations at both cysteins, which are very similar to a palmitoyl chain but very different from a farnesyl moiety. Although Cys 181 and 186 overlap in the spectrum and we therefore could only measure a mean order parameter for them, this order parameter is so low that it is impossible that the order parameter of Cys 186 is the highest of all amino acids as it was the case in the full-length protein. This supports the interpretation that the higher order parameter observed for Cys 186 in the full-length protein is due to the farnesyl lipid modification, which is less mobile than hexadecylations.

Another interesting result of the DIPSHIFT order parameter analysis is that Cys 181 and Met 182 whose conformations are highly mobile and most strongly correlated in the replica exchange simulation exhibit some of the lowest order parameters. This demonstrates the high flexibility of this part of the backbone and indicates that the transition between the two structures most commonly observed in the simulations must be faster than the timescale of the DIPSHIFT NMR experiment, which is on the order of tens of microseconds.

To obtain more detailed information on the correlation times of motion for each amino acid, T_1 and T_2 relaxation times were measured experimentally, interpreted in terms of a model free approach and compared to two independent conventional MD simulations of 300 ns length each. Overall, experiment and simulation show very good

agreement. Analysis of the experimental relaxation times using a modified Lipari–Szabo approach [44] describing two independent anisotropic motions of the peptide yields two correlation times. The obtained correlation times are very similar for all amino acids, where the fast motions are on the order of a few ns suggesting that these are internal motions such as isomerizations while the slow motions are on the order of hundreds of ns most likely describing overall reorientations of the peptide.

In general, the Ras membrane anchor is remarkably flexible and it is worthwhile to speculate about the biological relevance of this finding. As mentioned previously, the major differences in the individual Ras isoforms are located in the hypervariable region that includes the membrane anchor, which must, therefore, account for the differences in function. Previously, it has been shown that the localization of Ras at the membrane is crucial for its biological function [72] and it was shown by atomic force microscopy [73] and also ongoing investigations in our laboratory that human N-Ras tends to accumulate at the boundaries of membrane domains [76]. This region is characterized by complex dynamics [74] and associated with a line tension [75]. Therefore, from a biophysical perspective it can be understood that human N-Ras accumulates at these phase boundaries since due to its own complex dynamics it perfectly fits this environment and might in addition even lead to a reduction of the unfavorable line tension.

In summary, it can be concluded that the backbone of the membrane anchor of the human N Ras protein is characterized by a large degree of structural flexibility. Two dominant structures were found, which account for a combined ~60% of the simulation time and which are shaped by the biophysical interactions with the membrane. The backbone torsion angles of the amino acids Cys 181 and Met 182 are highly correlated, which is most crucial for the conformational flexibility of the Ras membrane anchor. All structures feature the same topology, in which the hydrophobic lipid modifications and side chains face one side of the peptide and penetrate the hydrocarbon core of the membrane, while the polar peptide backbone is located in the lipid water interface. The dynamics of the backbone is characterized by large amplitude motions which occur over a rather broad window of correlations times (up to hundreds of nanoseconds). Comparison to values obtained for the full-length Ras protein shows that its soluble part somewhat reduces the amplitude of motions of the membrane anchor but has little influence on their timescale. This work shows that combining solid-state NMR and MD simulations provides a very powerful approach to investigations on structure and dynamics of membrane proteins yielding a wealth of information not accessible by applying either method alone. In particular, the MD has shown how the torsion angles in the backbone are correlated, an information that cannot be revealed by TALOS alone. However, additional constraints such as NOEs or dipolar couplings could also reveal these correlations experimentally. Most importantly, we showed that the N-Ras membrane anchor exists in a dynamic ensemble of structures opposed to the case of single “frozen” structure as often obtained by various structural biology methods and in particular the correlation between conformations of different amino acids proved to be crucial to define the observed structures.

Acknowledgements

The authors would like to thank Dr. Richard M. Venable for providing the replica exchange package and Prof. Dr. Kay Saalwächter for helpful discussions about the evaluation of DIPSHIFT order parameters from MD. We thank the German Research Foundation (DFG) and the Experimental Physics Institutes of the Leipzig University for measuring time at Avance 750. The study was supported by the DFG (HU 720/10-1, VO 1523/1-1, and SFB 642) and the “Exzellenznetzwerk Biowissenschaften” funded by the federal state of Sachsen-Anhalt. SEF thanks the National Science Foundation for support under MCB-0543124.

References

[1] A.I. Bartlett, S.E. Radford, An expanding arsenal of experimental methods yields an explosion of insights into protein folding mechanisms, Nat. Struct. Mol. Biol. 16 (2009) 582–588.
[2] D.M. Korzhnev, X. Salvatella, M. Vendruscolo, A.A. Di Nardo, A.R. Davidson, C.M. Dobson, L.E. Kay, Low-populated folding intermediates of Fyn SH3 characterized by relaxation dispersion NMR, Nature 430 (2004) 586–590.
[3] D. Huster, L.S. Xiao, M. Hong, Solid-state NMR investigation of the dynamics of the soluble and membrane-bound colicin Ia channel-forming domain, Biochemistry 40 (2001) 7662–7674.
[4] G.E. Fanucci, J.Y. Lee, D.S. Cafiso, Membrane mimetic environments alter the conformation of the outer membrane protein BtuB, J. Am. Chem. Soc. 125 (2003) 13932–13933.
[5] P.M. Hwang, R.E. Bishop, L.E. Kay, The integral membrane enzyme PagP alternates between two dynamically distinct states, Proc. Nat. Acad. Sci. U. S. A. 101 (2004) 9618–9623.
[6] H. Saito, Dynamic pictures of membrane proteins in two-dimensional crystal, lipid bilayer and detergent as revealed by site-directed solid-state C-13 NMR, Chem. Phys. Lipids 132 (2004) 101–112.
[7] U.H.N. Durr, L. Waskell, A. Ramamoorthy, The cytochromes P450 and b(5) and their reductases—promising targets for structural studies by advanced solid-state NMR spectroscopy, Biochim. Biophys. Acta-Biomembr. 1768 (2007) 3235–3259.
[8] S.H. White, A.S. Ladokhin, S. Jayasinghe, K. Hristova, How membranes shape protein structure, J. Biol. Chem. 276 (2001) 32395–32398.
[9] D. Huster, K. Arnold, K. Gawrisch, Investigation of lipid organization in biological membranes by two-dimensional nuclear Overhauser enhancement spectroscopy, J. Phys. Chem. B 103 (1999) 243–251.
[10] A. Wittinghofer, H. Waldmann, Ras—a molecular switch involved in tumor formation, Angew. Chem. Int. Ed. 39 (2000) 4192–4214.
[11] A. Hall, A biochemical function for ras—at last, Science 264 (1994) 1413–1414.
[12] K.C. Hart, D.J. Donoghue, Derivatives of activated H-ras lacking C-terminal lipid modifications retain transforming ability if targeted to the correct subcellular location, Oncogene 14 (1997) 945–953.
[13] M.H. Gelb, L. Brunsveld, C.A. Hrycyna, S. Michaelis, F. Tamanoi, W.C. Van Voorhis, H. Waldmann, Therapeutic intervention based on protein prenylation and associated modifications, Nat. Chem. Biol. 2 (2006) 518–528.
[14] S.F. Sousa, P.A. Fernandes, M.J. Ramos, Farnesyltransferase inhibitors: a detailed chemical view on an elusive biological problem, Curr. Med. Chem. 15 (2008) 1478–1492.
[15] G.W. Reuther, C.J. Der, The Ras branch of small GTPases: Ras family members don't fall far from the tree, Curr. Opin. Cell Biol. 12 (2000) 157–165.
[16] I.A. Prior, J.F. Hancock, Compartmentalization of Ras proteins, J. Cell Sci. 114 (2001) 1603–1608.
[17] L. Brunsveld, H. Waldmann, D. Huster, Membrane binding of lipidated Ras peptides and proteins—the structural point of view, Biochim. Biophys. Acta 1788 (2009) 273–288.
[18] R.G. Parton, J.F. Hancock, Lipid rafts and plasma membrane microorganization: insights from Ras, Trends Cell Biol. 14 (2004) 141–147.
[19] O. Rocks, A. Peyker, P.I.H. Bastiaens, Spatio-temporal segregation of Ras signals: one ship, three anchors, many harbors, Curr. Opin. Cell Biol. 18 (2006) 351–357.
[20] H. Schroeder, R. Leventis, S. Rex, M. Schelhaas, E. Nagele, H. Waldmann, J.R. Silvius, S-Acylation and plasma membrane targeting of the farnesylated carboxyl-terminal peptide of N-ras in mammalian fibroblasts, Biochemistry 36 (1997) 13102–13109.
[21] B. Bader, K. Kuhn, D.J. Owen, H. Waldmann, A. Wittinghofer, J. Kuhlmann, Bioorganic synthesis of lipid-modified proteins for the study of signal transduction, Nature 403 (2000) 223–226.
[22] M. Baldus, Correlation experiments for assignment and structure elucidation of immobilized polypeptides under magic angle spinning, Prog. Nucl. Magn. Reson. Spectrosc. 41 (2002) 1–47.
[23] D. Huster, Investigations of the structure and dynamics of membrane-associated peptides by magic angle spinning NMR, Prog. Nucl. Magn. Reson. Spectrosc. 46 (2005) 79–107.
[24] G. Reuther, K.T. Tan, J. Kohler, C. Nowak, A. Pampel, K. Arnold, J. Kuhlmann, H. Waldmann, D. Huster, Structural model of the membrane-bound C terminus of lipid-modified human N-ras protein, Angew. Chem. Int. Ed. 45 (2006) 5387–5390.
[25] G. Reuther, K.T. Tan, A. Vogel, C. Nowak, K. Arnold, J. Kuhlmann, H. Waldmann, D. Huster, The lipidated membrane anchor of full length N-Ras protein shows an extensive dynamics as revealed by solid-state NMR spectroscopy, J. Am. Chem. Soc. 128 (2006) 13840–13846.
[26] G. Cornilescu, F. Delaglio, A. Bax, Protein backbone angle restraints from searching a database for chemical shift and sequence homology, J. Biomol. NMR 13 (1999) 289–302.
[27] Y. Shen, A. Bax, Protein backbone chemical shifts predicted from searching a database for torsion angle and sequence homology, J. Biomol. NMR 38 (2007) 289–302.
[28] S. Neal, A.M. Nip, H.Y. Zhang, D.S. Wishart, Rapid and accurate calculation of protein H-1, C-13 and N-15 chemical shifts, J. Biomol. NMR 26 (2003) 215–240.
[29] D. Huster, K. Kuhn, D. Kadereit, H. Waldmann, K. Arnold, ^{1}H high-resolution magic angle spinning NMR spectroscopy for the investigation of a Ras lipopeptide in a lipid membrane, Angew. Chem. Int. Ed. 40 (2001) 1056–1058.

[30] D. Huster, A. Vogel, C. Katzka, H.A. Scheidt, H. Binder, S. Dante, T. Gutberlet, O. Zschörnig, H. Waldmann, K. Arnold, Membrane insertion of a lipidated Ras peptide studied by FTIR, solid-state NMR, and neutron diffraction spectroscopy, J. Am. Chem. Soc. 125 (2003) 4070–4079.
[31] A.A. Gorfe, R. Pellarin, A. Caflisch, Membrane localization and flexibility of a lipidated ras peptide studied by molecular dynamics simulations, J. Am. Chem. Soc. 126 (2004) 15277–15286.
[32] T. Huber, K. Rajamoorthi, V.F. Kurze, K. Beyer, M.F. Brown, Structure of docosahexaenoic acid-containing phospholipid bilayers as studied by H-2 NMR and molecular dynamics simulations, J. Am. Chem. Soc. 124 (2002) 298–309.
[33] G.F. Salgado, R. Marquant, A. Vogel, I.D. Alves, S.E. Feller, N. Morellet, S. Bouaziz, Structural studies of HIV-1 Gag p6ct and its interaction with Vpr determined by solution nuclear magnetic resonance, Biochemistry 48 (2009) 2355–2367.
[34] L. Shi, A. Cembran, J.L. Gao, G. Veglia, Tilt and azimuthal angles of a transmembrane peptide: a comparison between molecular dynamics calculations and solid-state NMR data of sarcolipin in lipid membranes, Biophys. J. 96 (2009) 3648–3662.
[35] A. Lange, Z. Gattin, H. Van Melckebeke, C. Wasmer, A. Soragni, W.F. van Gunsteren, B.H. Meier, A combined solid-state NMR and MD characterization of the stability and dynamics of the HET-s(218-289) prion in its amyloid conformation, ChemBioChem 10 (2009) 1657–1665.
[36] S.V. Dvinskikh, K. Yamamoto, A. Ramamoorthy, Heteronuclear isotropic mixing separated local field NMR spectroscopy, J. Chem. Phys. (2006) 125.
[37] S.V. Dvinskikh, U.H.N. Durr, K. Yamamoto, A. Ramamoorthy, High-resolution 2D NMR spectroscopy of bicelles to measure the membrane interaction of ligands, J. Am. Chem. Soc. 129 (2007) 794–802.
[38] K. Hinterding, D. Alonso-Diaz, H. Waldmann, Organic synthesis and biological signal transduction, Angew. Chem. Int. Ed. 37 (1998) 688–749.
[39] E. Nagele, M. Schelhaas, N. Kuder, H. Waldmann, Chemoenzymatic synthesis of N-Ras lipopeptides, J. Am. Chem. Soc. 120 (1998) 6889–6902.
[40] M. Schelhaas, S. Glomsda, M. Hansler, H.D. Jakubke, H. Waldmann, Enzymatic synthesis of peptides and Ras lipopeptides employing choline ester as a solubilizing, protecting, and activating group, Angew. Chem. Int. Ed. 35 (1996) 106–109.
[41] M. Hong, J.D. Gross, R.G. Griffin, Site-resolved determination of peptide torsion angle phi from the relative orientations of backbone N–H and C–H bonds by solid-state NMR, J. Phys. Chem. B 101 (1997) 5869–5874.
[42] A. Bielecki, A.C. Kolbert, M.H. Levitt, Frequency-switched pulse sequences—homonuclear decoupling and dilute spin NMR in solids, Chem. Phys. Lett. 155 (1989) 341–346.
[43] P. Barre, O. Zschornig, K. Arnold, D. Huster, Structural and dynamical changes of the bindin B18 peptide upon binding to lipid membranes. A solid-state NMR study, Biochemistry 42 (2003) 8377–8386.
[44] G.M. Clore, A. Szabo, A. Bax, L.E. Kay, P.C. Driscoll, A.M. Gronenborn, Deviations from the simple two-parameter model-free approach to the interpretation of nitrogen-15 nuclear magnetic relaxation of proteins, J. Am. Chem. Soc. 112 (1990) 4989–4991.
[45] A.G. Palmer, J. Williams, A. McDermott, Nuclear magnetic resonance studies of biopolymer dynamics, J. Phys. Chem. B 100 (1996) 13293–13310.
[46] S. Jo, T. Kim, W. Im, Automated builder and database of protein/membrane complexes for molecular dynamics simulations, Plos One (2007) 2.
[47] H.I. Petrache, S.W. Dodd, M.F. Brown, Area per lipid and acyl length distributions in fluid phosphatidylcholines determined by H-2 NMR spectroscopy, Biophys. J. 79 (2000) 3172–3192.
[48] B.R. Brooks, R.E. Bruccoleri, B.D. Olafson, D.J. States, S. Swaminathan, M. Karplus, CHARMM—a program for macromolecular energy, minimization, and dynamics calculations, J. Comput. Chem. 4 (1983) 187–217.
[49] A.D. MacKerell, D. Bashford, M. Bellott, R.L. Dunbrack, J.D. Evanseck, M.J. Field, S. Fischer, J. Gao, H. Guo, S. Ha, D. Joseph-McCarthy, L. Kuchnir, K. Kuczera, F.T.K. Lau, C. Mattos, S. Michnick, T. Ngo, D.T. Nguyen, B. Prodhom, W.E. Reiher, B. Roux, M. Schlenkrich, J.C. Smith, R. Stote, J. Straub, M. Watanabe, J. Wiorkiewicz-Kuczera, D. Yin, M. Karplus, All-atom empirical potential for molecular modeling and dynamics studies of proteins, J. Phys. Chem. B 102 (1998) 3586–3616.
[50] A.D. MacKerell, M. Feig, C.L. Brooks, Improved treatment of the protein backbone in empirical force fields, J. Am. Chem. Soc. 126 (2004) 698–699.
[51] J.B. Klauda, B.R. Brooks, A.D. MacKerell, R.M. Venable, R.W. Pastor, An ab initio study on the torsional surface of alkanes and its effect on molecular simulations of alkanes and a DPPC bilayer, J. Phys. Chem. B 109 (2005) 5300–5311.
[52] U. Essmann, L. Perera, M.L. Berkowitz, T. Darden, H. Lee, L.G. Pedersen, A smooth particle mesh Ewald method, J. Chem. Phys. 103 (1995) 8577–8593.
[53] W.F. Vangunsteren, H.J.C. Berendsen, Algorithms for macromolecular dynamics and constraint dynamics, Mol. Phys. 34 (1977) 1311–1327.
[54] P. Maragakis, M. Spichty, M. Karplus, Optimal estimates of free energies from multistate nonequilibrium work data (vol 96, art no 100602, 2006), Phys. Rev. Lett. 98 (2007) 259901.
[55] K. Hukushima, K. Nemoto, Exchange Monte Carlo method and application to spin glass simulations, J. Phys. Soc. Jpn. 65 (1996) 1604–1608.
[56] Y.M. Rhee, V.S. Pande, Multiplexed-replica exchange molecular dynamics method for protein folding simulation, Biophys. J. 84 (2003) 775–786.
[57] P. Maragakis, M. Spichty, M. Karplus, Optimal estimates of free energies from multistate nonequilibrium work data, Phys. Rev. Lett. 96 (2006) 100602.
[58] C.H. Ye, R.Q. Fu, J.Z. Hu, L. Hou, S.W. Ding, Carbon-13 chemical shift anisotropies of solid amino acids, Magn. Reson. Chem. 31 (1993) 699–704.
[59] S.E. Feller, D. Huster, K. Gawrisch, Interpretation of NOESY cross-relaxation rates from molecular dynamics simulation of a lipid bilayer, J. Am. Chem. Soc. 121 (1999) 8963–8964.
[60] K. Schmidt-Rohr, H.W. Spiess, Multidimensional Solid-State NMR and Polymers, Academic Press, London, 1994.
[61] A. Vogel, K.T. Tan, H. Waldmann, S.E. Feller, M.F. Brown, D. Huster, Flexibility of ras lipid modifications studied by H-2 solid-state NMR and molecular dynamics simulations, Biophys. J. 93 (2007) 2697–2712.
[62] A. Vogel, C.P. Katzka, H. Waldmann, K. Arnold, M.F. Brown, D. Huster, Lipid modifications of a Ras peptide exhibit altered packing and mobility versus host membrane as detected by 2H solid-state NMR, J. Am. Chem. Soc. 127 (2005) 12263–12272.
[63] R. Thapar, J.G. Williams, S.L. Campbell, NMR characterization of full-length farnesylated and non-farnesylated H-ras and its implications for raf activation, J. Mol. Biol. 343 (2004) 1391–1408.
[64] R.M. Peitzsch, S. McLaughlin, Binding of acylated peptides and fatty acids to phospholipid vesicles: pertinence to myristoylated proteins, Biochemistry 32 (1993) 10436–10443.
[65] C.T. Pool, T.E. Thompson, Chain length and temperature dependence of the reversible association of model acylated proteins with lipid bilayers, Biochemistry 37 (1998) 10246–10255.
[66] C. Tanford, The Hydrophobic Effect: Formation of Micelles and Biological Membranes, John Wiley & Sons, New York, Chichester, Brisbane, 1980.
[67] H. Saito, T. Tsuchida, K. Ogawa, T. Arakawa, S. Yamaguchi, S. Tuzi, Residue-specific millisecond to microsecond fluctuations in bacteriorhodopsin induced by disrupted or disorganized two-dimensional crystalline lattice, through modified lipid-helix and helix-helix interactions, as revealed by C-13 NMR, Biochim. Biophys. Acta 1565 (2002) 97–106.
[68] L.A. Colnago, K.G. Valentine, S.J. Opella, Dynamics of Fd-coat protein in the bacteriophage, Biochemistry 26 (1987) 847–854.
[69] J.R. Silvius, F. l'Heureux, Fluorimetric evaluation of the affinities of isoprenylated peptides for lipid bilayers, Biochemistry 33 (1994) 3014–3022.
[70] T.J. Zahn, M. Eilers, Z.M. Guo, M.B. Ksebati, M. Simon, J.D. Scholten, S.O. Smith, R.A. Gibbs, Evaluation of isoprenoid conformation in solution and in the active site of protein-farnesyl transferase using carbon-13 labeling in conjunction with solution- and solid-state NMR, J. Am. Chem. Soc. 122 (2000) 7153–7164.
[71] A.C. Rowat, J.H. Davis, Farnesol-DMPC phase behaviour: a H-2-NMR study, Biochim. Biophys. Acta 1661 (2004) 178–187.
[72] S.J. Leevers, H.F. Paterson, C.J. Marshall, Requirement for Ras in Raf activation is overcome by targeting Raf to the plasma membrane, Nature 369 (1994) 411–414.
[73] K. Weise, G. Triola, L. Brunsveld, H. Waldmann, R. Winter, Influence of the lipidation motif on the partitioning and association of N-Ras in model membrane subdomains, J. Am. Chem. Soc. 131 (2009) 1557–1564.
[74] P.I. Kuzmin, S.A. Akimov, Y.A. Chizmadzhev, J. Zimmerberg, F.S. Cohen, Line tension and interaction energies of membrane rafts calculated from lipid splay and tilt, Biophys. J. 88 (2005) 1120–1133.
[75] S. Keller, A. Tsamaloukas, H. Heerklotz, A quantitative model describing the selective solubilization of membrane domains, J. Am. Chem. Soc. 127 (2005) 11469–11476.
[76] A. Vogel, G. Reuther, K. Weise, G. Triola, J. Nikolaus, K.-T. Tan, C. Nowak, A. Herrmann, H. Waldmann, R. Winter, D. Huster, The lipid modifications of ras sense the membrane environment and induce local enrichment, Angew. Chem. Int. Ed. 48 (2009) 8784–8787.